State-to-State Inelastic Scattering from S_1 Glyoxal with the Rare Gas Series: Uniform Rotational vs Changing Vibrational Channel Competition

Samuel M. Clegg, Andrew B. Burrill, and Charles S. Parmenter*

Department of Chemistry, Indiana University, Bloomington, Indiana 47405

Received: February 13, 1998; In Final Form: April 9, 1998

To provide data for the complete series of rare gases, relative cross sections are obtained for the crossed molecular beam state-to-state rotationally and rovibrationally inelastic scattering of S_1 (^1A_u) glyoxal (CHO−CHO) in its 0^0, $K' = 0$ states by Ne, Ar, and Xe. When added to cross sections from a new analysis of Kr data and to published data for H_2 and He, sets of cross sections for the entire rare gas series are available that show the competition among more than 25 rotational and rovibrational channels. The latter all involve $\Delta v_7' = +1$ where $\nu_7' = 233$ cm^{-1} is the lowest frequency mode. Despite large variations in the collisional kinematics and in the interaction potential energy surfaces, the competition among rotationally inelastic channels is essentially identical for the gases Ne, Ar, Kr, and Xe. In turn, those cases differ from H_2 and He solely by the fact that orbital angular momentum constraints with the light gases limit scattering to only those states with $\Delta K \lesssim 15$. In contrast, the competition between rotational and rovibrational scattering changes with the collision partner to the extent that state-to-state resolution of rovibrational scattering is not possible for Ar, Kr, and Xe. Previous theoretical predictions for Ar inelastic scattering are consistent with earlier arguments that this competition is dominated by kinematic factors rather than by variations in the interaction potential. The relative cross sections are obtained from experiments in which a laser prepares S_1 glyoxal in the 0^0 $K' = 0$ state with $J' \approx 0-10$. Dispersed S_1-S_0 fluorescence is used to monitor the inelastic scattering to more than 25 destination states with $\Delta K'$ resolution. Inelastic cross sections are extracted by computer simulation of the fluorescence spectra.

I. Introduction

The planar molecule glyoxal (CHO−CHO) with 12 vibrational degrees of freedom has provided an instructive experimental window on vibrational and rotational energy transfer. Perhaps no other polyatomic molecule has yielded such detailed information about the competition among such a large number of vibrational and rotational channels in single collisional encounters. The view comes from combining crossed molecular beams with a laser pump-dispersed fluorescence probe approach that not only allows selection of an initial rovibrational level from which energy transfer occurs but also permits observation of all important energy transfer channels.

So far, the studies have involved energy transfer from each of four initial rovibrational levels in the S_1 state encompassing three different modes.[1−5] For three of these initial levels, over 20 state-to-state channels are monitored. For the fourth level, the competition can be followed among almost 50 channels. The competition is seen experimentally by the sets of relative cross sections for the single-collision population of the destination states. The cross sections are extracted from the dispersed fluorescence by the use of spectral simulations.

Most of the glyoxal crossed beam experiments have involved the collision partners H_2 or He.[1−3] In the present paper, we report new results that allow the channel competition to be seen for the entire rare gas series, He to Xe. Since earlier work has shown that the internal degrees of freedom of the collision partner H_2 do not participate in the inelastic scattering,[5−8] we have also included H_2 in this rare gas series for the purpose of comparison.

Cross sections for inelastic scattering of glyoxal from the collision partners H_2, D_2, He, and Kr have been reported.[1−4]

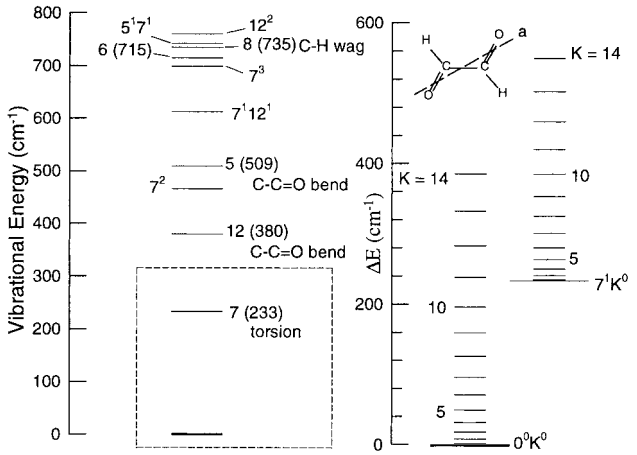

Figure 1. Some of the S_1 glyoxal energy levels that are accessible by inelastic scattering from the 0^0, $K' = 0$ level. (Left) All vibrational levels within 800 cm^{-1} of the S_1 zero point level. The frequency of fundamentals is given in parentheses. (Right) An experimental diagram showing K' rotational levels associated with the 0^0 and 7^1 vibrational states. The energies are those of states with $J' = K'$.

The results reported here come from new experiments that yield cross sections for Ne, Ar, and Xe. Additionally, we revisit the Kr data with an improved computer simulation in order to extract a more accurate set of cross sections. The end result is a characterization of the systematic changes that occur in the state-to-state channel competition when the collision partners range from H_2 to Xe.

Figure 1 displays most of the energy levels that are relevant to the present experiments. Glyoxal is a near-symmetric top

10.1021/jp981138v CCC: $15.00
Published on Web 06/06/1998

TABLE 1: Calculated Parameters for Glyoxal (0^0K^0) Collisions with H_2 or Rare Gases

target gas	μ^a ($\times 10^{-25}$ kg)	$v_{rel}{}^b$ ($\times 10^3$ m/s)	$E_{cm}{}^c$ (cm^{-1})	$\Delta K_{max}{}^d$ (via L)	$\Delta K_{max}{}^e$ (via E_{cm})
H_2	3.2	2810	640	14	18
He	6.2	2200	750	21	19
Ne	25	1520	1400	59	26
Ar	39	1420	2000	87	32
Kr	57	1350	2600	121	36
Xe	67	1340	3000	140	39

[a] Reduced mass of the system. [b] Relative velocity $v_{rel} = (v_1^2 + v_2^2)^{1/2}$. [c] Center of mass collision energy $E_{cm} = \mu v_{rel}^2/2$. [d] Limiting ΔK established by orbital angular momentum L. $\Delta K = \mu v_{rel} b/\hbar$. See Discussion. [e] Limiting ΔK established by E_{cm}. See Discussion.

($\kappa = -0.99$), and in the cold beam expansion ($\sim$35 K), it is possible to resolve the rotational K' states that define the angular momentum $L = K\hbar$ about the top axis (the "*a*" axis in Figure 1). A laser initially pumps the S_1 levels 0^0, $K' = 0$ with $J \lesssim 10$. For convenience, we refer to these initial states as 0^0K^0. The subsequent inelastic scattering of these excited molecules results in rotational excitation of higher K' states as well as the rovibrational states of the fundamental $\nu_7' = 233\ cm^{-1}$. Despite collision energies exceeding that of many other fundamentals, overtones, and combinations, excitation of this lowest frequency mode, the CHO−CHO torsion, is the only vibrational destination state that can be observed.

The resulting array of final states reached by the inelastic scattering fall in two groups, namely, those reached by pure rotational inelastic scattering and those associated with the ν_7' rovibrational scattering. These levels are observed in dispersed fluorescence that is isolated from only those molecules that have undergone inelastic scattering. The resolution (2 cm^{-1}) is sufficient to see the individual K' states. Relative cross sections for the inelastic scattering to the individual destination K' states are obtained by computer simulation of the dispersed fluorescence. Unfortunately J' state resolution is not possible, and little information is available concerning the excitation of overall rotational angular momentum described by the *J*-state distribution.

Glyoxal (0^0K^0) scattering has been reported earlier for H_2, D_2, He, and Kr.[1−5] Inelastic scattering fluorescence spectra have been reported for the collision partners N_2, CO, and C_2H_4, all 28 amu.[5] Additionally, scattering spectra of the pair C_6H_{12} (cyclohexane) vs Kr, both 84 amu collision partners, have been obtained at a reduced resolution (10 cm^{-1}), where the individual rotational channels could not be seen.[4] This ensemble of data displays trends that are further explored by the new data of the present study. Perhaps most intriguing is the recent discovery[5] that the details of the competition are much more responsive to the reduced mass of the collision pair than to variations of the intermolecular potential energy surface (PES). From this point of view, our exploration of glyoxal inelastic scattering by the rare gas series may be seen as a study of kinematic effects on rotationally and rovibrationally inelastic scattering. Such effects concern the relative velocity, center of mass collision energy, collisional linear momentum, impact parameter, and so forth. Some of the kinematic factors for our glyoxal + rare gas series are collected in Table 1. It is seen that they cover a wide range. Despite these variations, we will show that the competition among the inelastic scattering channels for the series has far more similarities than differences.

II. Experimental Procedures

A detailed description of the experimental apparatus and methods has been published,[3,9] and only a brief description of the beam conditions and experimental apparatus is given here. The experiment involves two molecular beams, a seeded glyoxal beam crossed at 90° with a rare gas target beam. The seeded beam is prepared by passing 160 Torr of helium over solid glyoxal maintained at −25 °C, producing approximately a 7% glyoxal in helium mixture. This beam is generated by expansion from a General Valve pulsed nozzle with a 0.5 mm diameter orifice. The beam is skimmed to narrow the collision region and to better define the collision conditions. The target beam consists only of the inert gas neon, argon, or xenon. This beam is produced by the expansion of approximately 20 Torr of the target gas from a second General Valve pulsed nozzle with a 0.5 mm diameter orifice and is unskimmed.

The molecular beam velocities are estimated from the expansion conditions. The sample beam velocity has been estimated assuming zero velocity slip between the glyoxal and the He carrier gas. As discussed elsewhere,[1,9] the molecular beam velocity will tend toward the isentropic limit, $v_{isen} = (2C_p' T/m')^{1/2}$, where C_p' is the molar averaged heat capacity, T is the stagnation temperature 300 K, and m' is the molar averaged mass. This assumption yields a maximum glyoxal velocity of 1.3×10^5 cm/s. The target beam velocity should be close to that derived from the monotonic gas formula, $v = (5kT/m)^{1/2}$, where k is the Boltzmann constant, T is the stagnation temperature 300 K, and m is the mass of the target gas. Table 1 lists the calculated velocity of each target gas as well as the collision energy, $E_{cm} = \mu(v_1^2 + v_1^2)/2$, as obtained with the calculated velocities.

Under our experimental conditions, most of the inelastically scattered glyoxal molecules are involved in only a single collision. This situation is achieved by adjusting the target gas expansion so that only 15−25% of the excited glyoxal molecules are involved in inelastic collisions. Since the probability of a scattered molecule encountering a second collision is the same as the probability of the first, 75−85% of the inelastically scattered glyoxal molecules encounter only a single collision.

A 10 Hz pulsed laser with a 0.3 cm^{-1} bandwidth is used to pump glyoxal into the 0^0, $K' = 0$ states with $J' = 0-10$. The pumping is achieved by tuning to the $K' = 0 \leftarrow K'' = 1\ 0_0^0$ glyoxal sub-bandhead at 455.05 nm.[3]

All of the important inelastic scattering channels are monitored by S_1-S_0 fluorescence. Some of the fluorescence is directed into a 1.7 m monochromator, where the dispersed fluorescence is collected by a photomultipler tube (PMT). The monochromator resolution of 2 cm^{-1} is sufficient to resolve ^rR sub-bandheads. The dispersed fluorescence signal is normalized on a shot-to-shot basis to the total fluorescence intensity as monitored with a second PMT. Two spectra are recorded on alternate laser shots: a collision free spectrum where only the sample nozzle fires and a spectrum where both nozzles fire. Emission from only those states populated by inelastic scattering emerges from the subtraction of the two spectra. Three point smoothing of the resulting spectra is used to reduce the noise.

III. Results and Analysis

The experimental data consist of dispersed S_1-S_0 emission that originates only from those S_1 glyoxal molecules that have undergone inelastic scattering. These scattering spectra, as we term them, are obtained as the difference between spectra generated with and without the target beam running. Characterization of the inelastic scattering is given by the relative state-to-state cross sections that are extracted from computer simulations of the scattering spectra.

A. Inelastic Scattering Spectra. A segment of the scattering spectrum from glyoxal + Ne is displayed in Figure 2. It

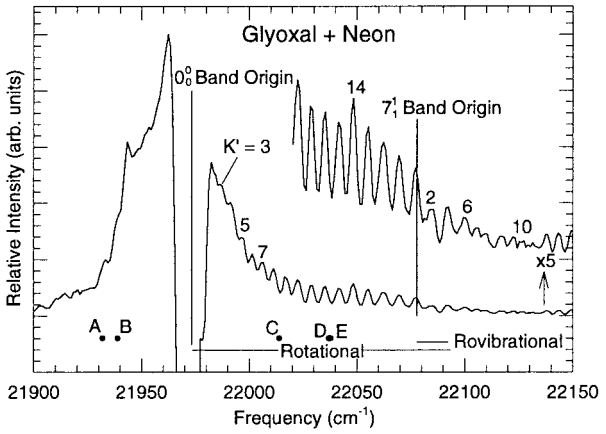

Figure 2. Segment of the fluorescence spectrum from S_1 glyoxal molecules that have been inelastically scattered by Ne. The structure is from states within the 0^0 level populated by rotationally inelastic scattering and from states within the 7^1 level reached by rovibrational scattering. The gap at the 0_0^0 band origin is due to depopulation of the initially pumped states. The maxima to the blue of the 0_0^0 origin are ^{r}R sub-bandheads from K' states populated by the inelastic scattering. Some are labeled with the K' identity. Labels to the blue of the 7_1^1 origin are for K' states associated with the 7^1 vibrational states. The region to the blue of the 22 020 cm^{-1} is displayed with 5× enhancement and displaced for clarity. The calculated positions of the 0_0^0 band origins at 21 973 cm^{-1} and the 7_1^1 origin at 22 078 cm^{-1} are marked. The origin positions are also marked for other bands: A(5_1^1), B(7_2^2), C(12_1^1), D(7_3^3), and E($5_1^17_1^1$).

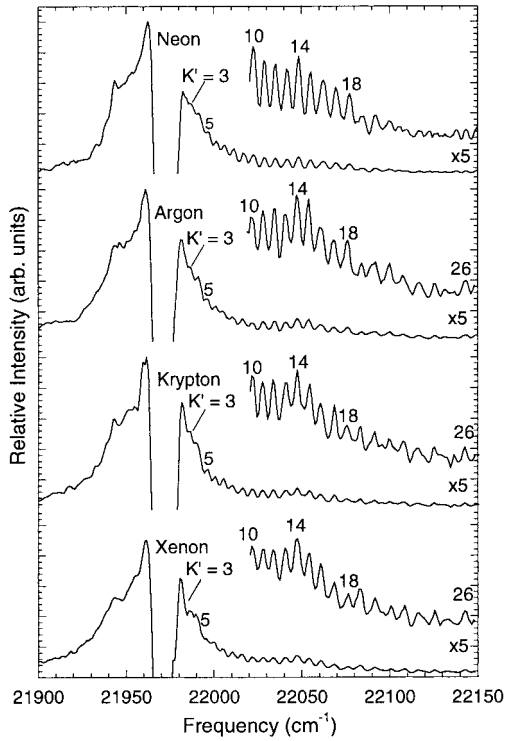

Figure 3. Segments of scattering spectra for glyoxal (0^0K^0) + Ar, Kr, and Xe in a display analogous to that in Figure 2. The Ne spectrum of Figure 2 is included for comparison. All of the K' notations refer to ^{r}R sub-bandheads of the 0_0^0 band and involve states populated by rotationally inelastic scattering.

includes emission from states reached by both rotational and rovibrational inelastic scattering. The gap in the 0_0^0 band origin region is a result of depopulation of the initially pumped 0^0K^0 states. The maxima to the blue are ^{r}R sub-bandheads from the $0^0K'$ destination states reached by rotationally inelastic scattering, some of which are labeled by the K' value. The only rovibrational inelastic scattering channel that contributes to the structure involves $\Delta v_7 = +1$. That structure is associated with the 7_1^1 band, and some of the $7^1K'$ states responsible for the ^{r}R sub-bandheads to the blue of the 7_1^1 origin are labeled in the figure.

All of the vibrational states included in the level diagram of Figure 1 are energetically accessible by rovibrational scattering, and strong emission bands from five would occur within the spectral range of Figure 2, namely, 12^1, 7^2, 5^1, 7^3, and 5^17^1. The band origin positions are marked on the figure. None of the bands is detectable. Since it is unlikely that any of the other levels would be associated with larger rovibrational cross sections, we conclude that $\Delta v_7 = +1$ scattering is the only significant rovibrational channel in glyoxal + Ne interactions. There is some indication that an additional rovibrational channel is active in collisions with the heavier target gases. The issue is addressed below.

The analogous scattering spectra for glyoxal + Ar, Kr, and Xe are displayed in Figure 3 with the Ne spectrum included for comparison. The Kr spectrum has been published previously,[4] but it appears here with revised $0^0K'$ assignments as a consequence of an improved spectral analysis.

B. Spectral Simulation and the Relative Scattering Cross Sections. The state-to-state cross sections are extracted from the scattering spectra by computer simulation. Details of the simulation program are given elsewhere.[3] So much is known about the spectroscopy and photophysics of glyoxal that the spectrum can be simulated with essentially only two adjustable parameters. One is associated with the profile of the sub-bandheads. We model those maxima by use of an effective J distribution $P(J)$ in the destination states that has the form

$$P(J) = (2J + 1)e^{-BJ(J+1)/kT}$$

in which J runs from K' to 100 and $T = 100$ K. We attach no physical significance to our chosen $P(J)$; it is merely a convenient way to model the width and depth of the sub-bandhead maxima.

The second parameter is the set of relative destination state populations. Since the scattering is essentially a single-collision event under our beam conditions, these populations are also the relative state-to-state cross sections that we seek. Comments about the small influence of multiple collisions have been given elsewhere.[5]

The changes to our original spectral fitting program for the present analysis involve the rotational term values. Glyoxal is almost a symmetric top ($\kappa = -0.99$), and the term values are approximated as such. Specifically,

$$F(J,K) = J(J+1)B + (A - B)K^2 - D_J\,(J(J+1))^2 - D_{JK}\,J(J+1)K^2 - D_K K^4$$

The last three terms account for centrifugal distortion and were ignored in our previous spectral simulations because of their small contributions to the rotational energies. Now, with our use of heavier collision partners that populate higher K' states, they become important. The zero point centrifugal distortion constants are, in cm^{-1}, $D_J' = 6.1 \times 10^{-6}$, $D_J'' = 6.2 \times 10^{-6}$, $D_{JK}' = D_{JK}'' = -8.4 \times 10^{-5}$, $D_K' = 3.2 \times 10^{-3}$, and $D_K'' = 1.9 \times 10^{-3}$.[10] It is, however, the excited state vs ground state differences that affect line positions. While ΔD_J and ΔD_{JK} are small enough to be ignored, ΔD_K is not, and since the constant is multiplied by K^4, its inclusion is important for the higher K'

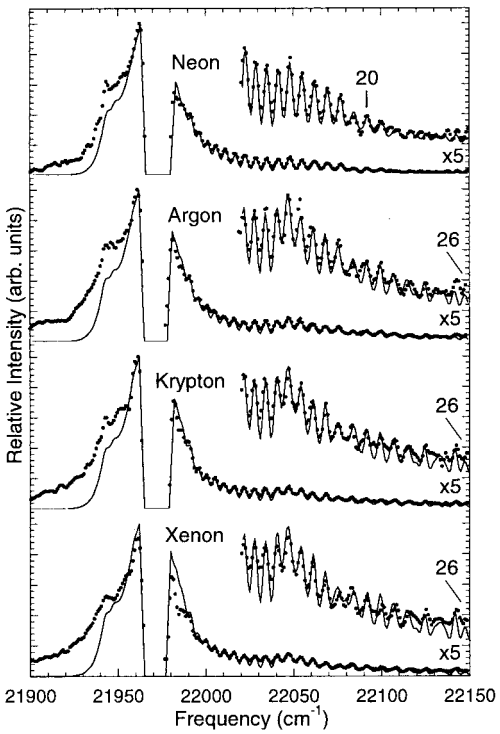

Figure 4. Comparison of the experimental scattering spectra (dots) with the best fit computer simulation (solid line) for glyoxal (0^0K^0) + Ne, Ar, Kr, and Xe.

states produced by the heavy collision partners. Adding the D_KK^4 contributions to the term values shifts the sub-bandheads increasingly to the red as K' increases.

Inclusion of centrifugal distortion does not affect our earlier analysis of glyoxal + H_2 and glyoxal + He spectra.[1−3] In those cases, the highest K' values reached by inelastic scattering, $K' = 14$ or 15, are not enough to allow the centrifugal distortion corrections to be meaningful relative to our experimental resolution. As the target gas mass and collision energies increase, observable rotational excitation extends to K' states as high as 26, and the addition of centrifugal distortion corrections become important for a proper accounting of the spectral structure.

Comparisons between the simulated and experimental scattering spectra for glyoxal + Ne, Ar, Kr, and Xe are shown in Figure 4. An earlier simulation of the glyoxal + Kr spectrum without correction for centrifugal distortion has been presented elsewhere.[4] Comparisons of the two simulations reveal the marked improvement provided by the new simulation, especially at the blue end where emission from high $0^0K'$ states occurs.

The simulations of the glyoxal + H_2 and He spectra[1−3] were relatively straightforward on account of a separation that exists between emission from states reached by rotational scattering and that from rovibrational scattering. Since there was little spectral overlap, all of the sub-bandheads from these scattering events could be resolved, and accordingly, the relative cross sections for all of the $0^0K'$ and $7^1K'$ destination states shown in Figure 1 were extracted without ambiguity.

The spectral simulations are more difficult for Ne, and the difficulty increases further for the heavier scattering gases. The complication arises on account of rotational scattering to higher $0^0K'$ states whose emission structure overlaps that of the $7^1K'$ states reached by rovibrational scattering. With Ne, $0^0K'$ states with $K' = 20$ are important contributors to the emission structure, and with all the heavier gases, the $0^0K'$ structure continues to at least $K' = 26$. It would be instructive to see the high ΔK tails of rotational inelastic scattering by the heavy gases, but it is beyond the limit of our experimental sensitivity. Centrifugal distortion corrections are important for all these gases, but additionally, care must be taken to identify properly the contributions of rotational vs rovibrational inelastic scattering to the overlapping structure.

In the Ne scattering spectrum, the series of sub-bandheads from the 0^0K^{18-20} states overlaps sub-bandheads from the 7^1K^{0-6} states. In these cases, it is important to fit the shape of the peak as well as the height to extract the individual contributions. Simulations of these overlapping maxima could accommodate various mixtures of the contributing state populations, and this ambiguity is reflected in larger error bars on some of the relative cross sections.

Simulations of the Ar, Kr, and Xe spectra reveal that all the structure to the blue of the 0_0^0 gap is due to emission from $0^0K'$ states populated by rotational scattering. This emission persists at least to $K' = 26$. The sub-bandheads from this scattering are sufficiently intense that all structure from the $7^1K'$ states reached by rovibrational scattering is obscured. As opposed to the case of glyoxal + Ne, there is no indication based on the shape of the $0^0K'$ sub-bandheads of any contributions to the structure from rovibrational scattering. Consequently, state-to-state rotationally inelastic cross sections for Ar, Kr, and Xe are reported only for rotationally inelastic scattering.

While structure from rovibrational scattering to the $7^1K'$ states cannot be resolved in the heavy gas scattering spectra, the presence of rovibrational scattering remains much in evidence. It appears as the hump underlying structure in the region 22 040−22 080 cm^{-1}, a consequence of the buildup of the 7^1 ^pP sub-bandhead structure. (The analogous structure from $0^0K'$ states occurs to the red of the 0_0^0 band gap.) Emission from the $7^1K'$ states reached by the rovibrational channel was included in the glyoxal + Ar, Kr, and Xe simulations. While there is no evidence in the simulations that the positions of any maxima in this region are affected by the underlying $7^1K'$ emission, the relative intensities of the maxima cannot be reasonably reproduced without this rovibrational emission. For the spectral simulation, the $7^1K'$ populations were initially assumed to have a distribution equivalent to that of glyoxal + Ne scattering. The distribution was then modestly adjusted to fit the bottom of the wells between the sub-bandheads. This fitting gave the simulations for glyoxal + Ar, Kr, and Xe that is shown in Figure 4. It provides an upper limit to the rovibrational cross sections.

One can argue that the distribution of $7^1K'$ cross sections so obtained is over estimated relative to the distribution of rotational cross sections derived from fitting the maxima with $0^0K'$ emission. The argument centers on the fact that our simulations for all scattering gases consistently produce poor fits to the intensity to the red of the 0_0^0 band gap (see Figure 4). The intensity in this region is due primarily to overlap of ^pP sub-bandheads from the $0^0K'$ states. Increasing the rotational cross section for the $0^0K'$ states for $K' = 12-26$ improves the fit in this red region but overestimates intensity in the blue ^rR sub-bandhead region. To compensate, the magnitude of $7^1K'$ cross sections may be decreased. This compromise results in a poorer fit of the well depths and of the ^rR sub-bandhead profiles. We use the fit, however, as our lower bound to the rovibrational cross sections.

There are indications that inelastic scattering from Ar, Kr, and Xe might excite an additional vibrational channel, namely, 12^1. The 12^1 vibrational mode is a C−C═O bend 380 cm^{-1} above the zero point level, and the 12_1^1 band origin is within the range of our spectra (see Figure 2). Inclusion of this

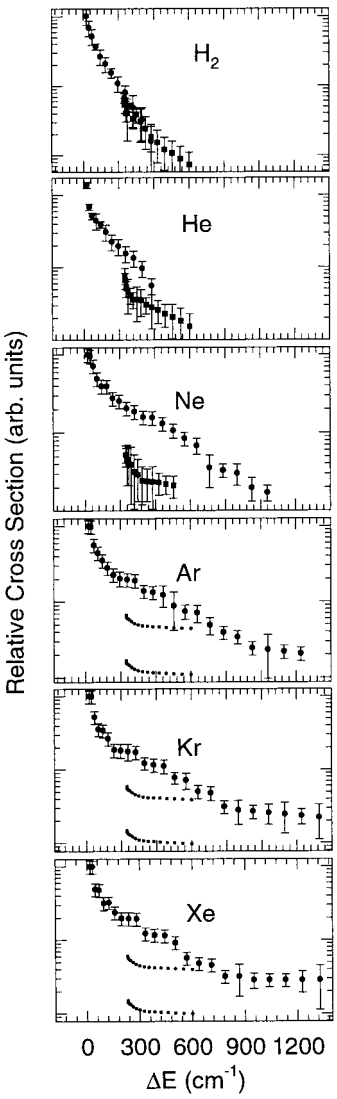

Figure 5. Relative cross sections for inelastic scattering of glyoxal (0^0K^0) by H_2 and the rare gases plotted against ΔE, the $T \rightarrow R, V$ energy transferred. For H_2, He, and Ne, rotationally and rovibrationally inelastic cross sections are shown with circles and squares, respectively, as well as with error bars. For Ar, Kr, and Xe, only rotationally inelastic cross sections are shown. The dashed lines show the upper and lower bounds for vibrational cross sections.

scattering channel resulted in a fit that more closely simulated the valleys between the ^rR sub-bandheads in the region from 22 000 to about 22 050 cm^{-1}. According to the simulations, this channel cannot exceed 7% of the total inelastic scattering cross section, and it may be much less. Earlier theoretical calculations[3,7] for the lighter target gases, H_2, He, and Ar predicted that 12^1 is an active but small scattering channel. In the predictions, the channel accounted for no more than 1% of the total cross section.

The relative cross sections for Ne, Ar, Kr, and Xe are listed in Table 2 and plotted against the energy transferred, ΔE, in Figure 5. Relative cross sections for H_2 and He have been given elsewhere.[3] Sets for the various gases are not normalized to one another, and no information has been obtained from the data about the absolute magnitudes of these cross sections. The Ne cross sections include those for both rotationally inelastic scattering, identified by the destination states $0^0K'$, and rovibrational scattering to the destination states $7^1K'$. As described above, only the rotational cross sections for Ar, Kr, and Xe can be extracted from the scattering spectra. Maximum and minimum ranges for rovibrational cross sections emerge from the analysis without the individual state-to-state values. These ranges are indicated on the cross section plots of Figure 5.

TABLE 2: Relative Inelastic Scattering Cross Sections for Glyoxal (0^0K^0) with Various Collision Partners[a]

	Ne		Ar	Kr	Xe
K'	$0^0K'$	$7^1K'$	$0^0K'$	$0^0K'$	$0^0K'$
0		0.052			
1		0.052			
2		0.045			
3	[1.0]	0.04	[1.0]	[1.0]	[1.0]
4	0.96	0.04	0.99	0.99	0.91
5	0.70	0.03	0.58	0.52	0.49
6	0.49	0.03	0.47	0.37	0.48
7	0.39	0.02	0.35	0.34	0.32
8	0.38	0.02	0.29	0.27	0.32
9	0.26	0.02	0.23	0.20	0.24
10	0.26	0.02	0.20	0.19	0.20
11	0.21	0.02	0.20	0.18	0.20
12	0.19	0.02	0.19	0.18	0.19
13	0.16	0.02	0.14	0.12	0.12
14	0.16	0.01	0.13	0.12	0.12
15	0.13		0.12	0.12	0.11
16	0.11		0.09	0.07	0.09
17	0.08		0.07	0.07	0.06
18	0.07		0.07	0.05	0.05
19	0.04		0.05	0.05	0.05
20	0.03		0.04	0.03	0.03
21	0.03		0.03	0.03	0.03
22			0.03	0.03	0.03
23			0.02	0.03	0.03
24			0.02	0.03	0.03
25			0.02	0.02	0.03
26			0.02	0.02	0.03

[a] Cross sections for rotational scattering are identified by the destination states $0^0K'$ and those for rovibrational scattering by the destination states $7^1K'$. The values have been normalized to unity for the 0^0K^3 cross section for each gas.

There are several sources of potential uncertainty associated with these experiments. Details of these uncertainties are discussed elsewhere.[3] It is believed that the primary source of uncertainty arises from the subjective nature of fitting the spectra, and it is only this type of error that is reflected in the error bars. Determination of the error bars involved increasing and decreasing the value of each individual cross sections until the simulation became visually unacceptable.

IV. Discussion

This study of single-collision inelastic scattering of S_1 glyoxal by the rare gases focuses on the competition among at least 25 channels. As described in the Introduction and shown in Figure 1, these channels involve pure rotationally inelastic scattering from the initial S_1 glyoxal state 0^0K^0 and rovibrational inelastic scattering that excites specific rotational states in the lowest vibrational level, $\nu_7' = 233$ cm^{-1}.

The competition is seen most fundamentally in the segment of S_1-S_0 fluorescence spectra shown in Figures 2 and 3 that include the 0_0^0 band comprised of emission from the states 0^0, $K' = n$ reached by rotational scattering and the 7_1^1 band comprised of emission from the states 7^1, $K' = n$ populated by rovibrational scattering. The competition is seen more explicitly in Figure 5, where the sets of relative cross sections are displayed for each target gas. The cross sections are derived from simulations of the fluorescence spectra. For convenience, we label the state-to-state cross sections according to the identity of the destination state. Thus, rotationally inelastic cross

sections are designated $\sigma(0^0K^n)$, and those for rovibrationally inelastic scattering are labeled $\sigma(7^1K^n)$.

An earlier comparison of inelastic scattering with H_2, D_2, and He[5] suggests that the H_2 and D_2 internal degrees of freedom do not observably participate in the inelastic scattering. Hence, the previously obtained cross sections for H_2 are included with those for He to set up a discussion of scattering with the entire "rare gas" series H_2, He, Ne, Ar, Kr, and Xe.

A. Rotational vs Rovibrational Inelastic Scattering Competition. The cross sections displayed in Figure 5 show immediately the dominant aspect of the competition between rotationally and rovibrationally inelastic scattering. The magnitude of the rotational scattering increases relative to vibrational scattering as the mass of the target gas increases. The increasing dominance of rotational scattering is, in fact, sufficient to preclude measurement of individual state-to-state rovibrational cross sections for the heavier gases Ar, Kr, and Xe.

We long ago noted the surprising similarity of rotational and rovibrational scattering of H_2 from glyoxal (0^0K^0) for comparable energy transfer.[1,3] As seen in Figure 5, the rotational and rovibrational cross sections merge smoothly when plotted against ΔE, the energy transferred $T \rightarrow V,R$, in the inelastic scattering. In contrast, the cross sections of He scattering[2,3] show the expected separation between the rotational and rovibrational sets. Our new data for Ne scattering now show that this separation increases. As displayed in Figure 5, the competition is only poorly seen for Ar, Kr, and Xe, suggesting that the separation has grown further for the heavier collision partners.

Elsewhere[5] we have commented on the relative importance of the interaction PES vs the collisional kinematics in establishing these distinctive competitions. Observations of inelastic scattering with the trio of collision partners H_2 vs D_2 vs He, where D_2 and He cross sections are the same, strongly suggest that the collisional kinematics play the dominant role in the competition. This conclusion is reenforced by experiments with a trio of 28 amu collision partners, N_2 vs CO vs C_2H_4, for which the channel competition is almost identical despite the large differences in potential energy surfaces.

Presumably, kinematics are playing a similarly dominant role in the channel competition for the entire rare gas series. Experiments are now underway to instruct us about which aspects of kinematics are most important.[5] The center-of-mass collision energy, the relative velocity, and the collision momentum can all be controlled experimentally in order to illuminate this issue.

Three-dimensional fully quantal inelastic close-coupled infinite-order-sudden-scattering calculations designed for our beam conditions have been reported for the collision partners H_2[6−8] and He.[7,11] Comparisons between the predicted and experimental cross sections are included in Figure 6. Since the calculations used an identical interaction PES for both gases derived from ab initio treatment of S_0 formaldehyde + He,[6−8,11] the impressive match for H_2 and He further emphasizes the secondary role of the PES in controlling the competition.

The only theoretical predictions relevant to our new rare gas data concern the collision partner Ar.[7] They are shown in Figure 6. Scattering calculations for glyoxal (0^0K^0) + Ar collisions are available for E_{cm} = 80 meV (650 cm^{-1}) collisions as opposed to our experimental E_{cm} = 250 meV (2000 cm^{-1}). The calculations are based on an intermolecular PES adapted from ab initio calculations on the S_0 formaldehyde + Ar interaction. Despite the large E_{cm} mismatch and the approximate PES, the comparison in Figure 6 shows that the experimental and predicted rotational distributions agree remarkably well over the limited ΔE range of comparison (see comments below). In contrast, the experimental and predicted rovibrational values differ by about an order of magnitude. We take this mismatch as further indication of the kinematic dominance of the rotational vs rovibrational competition. Given the consistent agreement between the theory and experiment whenever the E_{cm} assumed for calculation is that of the experiment, the singular mismatch in Figure 6 is almost certainly due to the low E_{cm} used in the calculation.

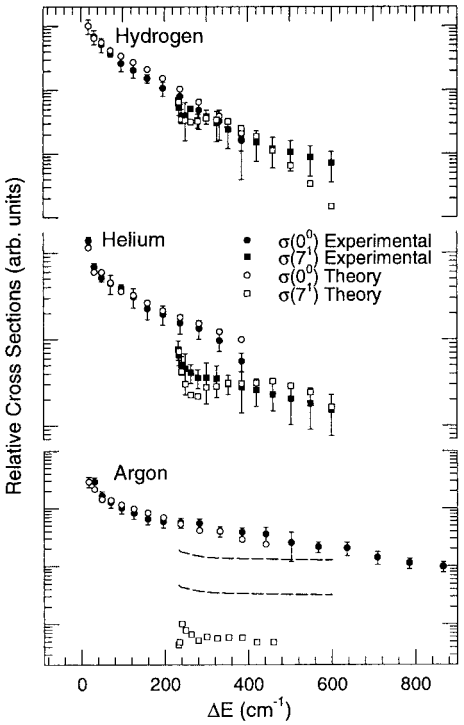

Figure 6. Plot of predicted (open symbols) and experimental cross sections (solid symbols or dashed lines) for inelastic scattering of glyoxal (0^0K^0) by H_2, He, and Ar against the energy transferred, ΔE. The H_2 and He cross sections are from ref 3 (experimental) and refs 8 and 11 (predicted). The predicted Ar cross sections are from ref 7.

B. Distributions of Rotationally Inelastic Scattering Cross Sections. Plots of the rotationally inelastic cross sections are presented in Figure 7 to show the most compelling aspect of the scattering. When the relative rotational cross sections are plotted against ΔE or ΔK with common normalization, the cross section distributions for H_2 and all the rare gases generally match to within the error bars. Thus, the channel competitions in rotationally inelastic scattering of glyoxal (0^0K^0) by these gases all look much the same. The only deviations from this common behavior are small, occurring at the very tail end of scattering by H_2 and He (large ΔE or large ΔK). We emphasize that it is the cross section distributions that match, not the absolute cross sections themselves. While the absolute values cannot be extracted from our spectra, we presume they differ substantially among the rare gases.

The close match of rotational distributions is further emphasized by comparisons of the original scattering spectra for the heavier gases Ar, Kr, and Xe. In these cases, the fluorescence contributions of states populated by rovibrational scattering is so small that the spectra represent fairly good views of rotationally inelastic scattering alone. Figure 8 displays the spectra normalized to one another. The relative populations of rotational states within the 0_0^0 band control the relative intensities of the structure, and in the superposition of the spectra in Figure 8, it is seen that those populations must be remarkably similar.

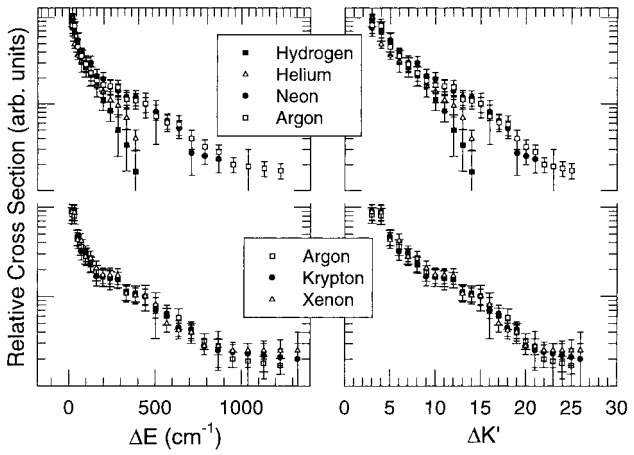

Figure 7. Plots of the relative cross sections for rotationally inelastic scattering of glyoxal (0^0K^0) by H_2 and the rare gases. The sets of cross sections have been normalized to one another for comparisons. They are presented in two groups for clarity with cross sections for Ar shown with both groups. One display shows the cross sections plotted against ΔE, the energy transferred $T \rightarrow R$. The other shows the cross sections plotted against $\Delta K'$, a measure of the transfer of orbital angular momentum to internal angular momentum.

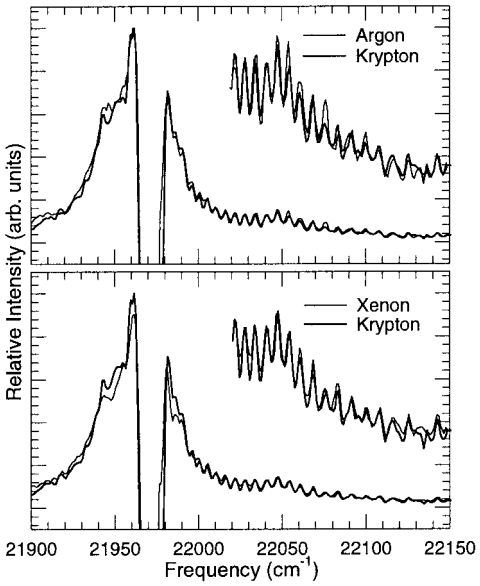

Figure 8. Superposition of the scattering spectra from glyoxal (0^0K^0) in collision with Ar, Kr, and Xe. The intensities of the three spectra have been normalized to one another, and the superpositions are presented pairwise for clarity. The spectra are those from Figure 3.

The qualitative similarity of cross section distributions for energy transfer about the top axis of glyoxal is far from a unique situation. Common cross section distributions among rare gas partners appears to be the rule rather than the exception for diatomic molecules in thermal systems. The central interest in the diatomic studies has generally concerned the development of fitting or scaling laws to accommodate absolute cross sections. Hence, the existence of common distributions has been acknowledged only implicitly in the literature. One can see, however, the near coincidence of distributions for a given set of rotational cross sections from a specific level in a diatomic by the close match of fitting or scaling law parameters for various rare gas collision partners. More explicitly, the coincidence of cross section distributions emerges clearly when normalized plots of the absolute cross sections are made in a form similar to those of Figure 7. We have made such comparisons from the reported data for numerous diatomic

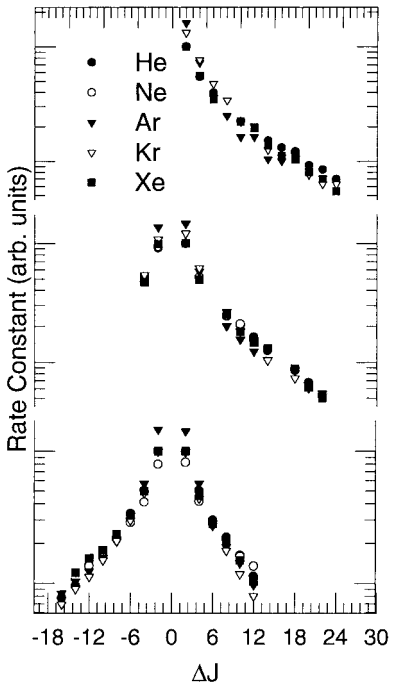

Figure 9. Rate constants for state-to-state rotational energy transfer from $J = 4$, $J = 6$ and $J = 38$ of A(Σ) Na_2 in collision with He, Ne, Ar, Kr, or Xe plotted against ΔJ. The sets of cross sections for various gases have been normalized to one another for each initial state. The data are from ref 24.

molecules, usually in excited electronic states. The diatom−atom systems include I_2 with He,[12,13] Kr,[13] and Xe;[12] Li_2 with Ne, Ar, and Xe;[14] NO with He,[15−18] Ne,[16] Ar,[15−18] and Kr;[16] HF with He, Ne, and Ar;[19] CN with He[20] and Ar;[21] and IF with He, Ne, Ar, Kr, and Xe.[22,23] As with glyoxal, the distributions for the heavier rare gases for a given diatomic generally match qualitatively over an extended ΔJ range, where as that for He often falls off at large ΔJ. This He fall off has usually been attributed to angular momentum constraints.

The most extensive diatomic data are probably those of Na_2 that include the entire rare gas series of collision partners.[24−30] To bring emphasis to the generally unrecognized existence of common rotational distributions that occur in many diatomic systems, we display in Figure 9 some of the Na_2 data[24] plotted in a form that reveals the close similarity of the rate constant distributions among the entire set of rare gas collision partners.

To quote a recent review, "state-resolved rotational energy transfer in polyatomic molecules is a relatively unstudied arena".[31] With respect to finding polyatomic data that yield cross section distributions for comparison among rare gas collision partners, this lament rings true. We have been able to find suitable data only for CH_4 and NH_3. The motivations for studying rotational transfer with these molecules are often associated with making connections to the interaction PES, and explicit comparisons of the distributions are not given in the literature. Our explorations of the data for CH_4 with He,[32,33] Ne,[33,34] and Ar[33,35−37] show that the situation is much the same as that for the diatomic systems and for glyoxal. The distributions for the heavier rare gases are qualitatively similar, whereas that for He[33] is somewhat distinct. The initial efforts for NH_3 involved explorations of the selection rules using He, Ar, and Xe.[38,39] Subsequently, absolute cross sections become available for Ar from bulb experiments,[40] and relative cross sections became available for H_2,[41,42] He,[41] and Ar[43] from crossed beam experiments. Whereas the bulb cross sections may be fitted

with an exponential gap law (EGL),[40] the distributions for the various rare gas partners differ from each other.

As noted above, the competition between rotationally and rovibrationally inelastic scattering in glyoxal is controlled predominantly by kinematic factors. The secondary role of the interaction PES is ascribed to the fact that the interactions are dominated by the repulsive wall of the PES and that these steep walls do not differ greatly even among collisional systems, even though other regions of the PES may differ substantially.

One presumes that this rationale also pertains to the rare gas collision partners associated with our rotational cross section distributions. The rotationally inelastic scattering in our crossed beam experiments involves impulsive interactions with the repulsive wall, and presumably neither the anisotropy nor the steepness of the wall differs enough among the rare gas partners to produce unique rotationally inelastic scattering distributions. The narrow range of parameters that characterize the PES associated with the scaling and fitting laws for the diatomic systems are consistent with this proposition. It is further reenforced by the narrow range of PES parameters derived from the highly successful use of a recent angular momentum model[44,45] that reproduces quantitatively many of the diatomic cross sections.

An intriguing dichotomy arises concerning the kinematic factors that prove so important in controlling the rotational vs rovibrational inelastic scattering competition. Since the kinematics have such a large influence on that competition, the question then arises as to why the rotational distributions are not also responsive to the kinematic differences. Those distributions remain impressively insensitive to kinematic variations. The situation may be put in perspective by noting the broad range of collisional parameters that exist in our glyoxal−rare gas series. Differences in the kinematic factors, as displayed in Table 1 or inferred from its entries, span as much as an order of magnitude. The question concerns such a universal aspect of rotational energy transfer in both diatomic and polyatomic molecules that it warrants explicit theoretical attention. For example, insights might emerge from further explorations of the angular momentum model[44,45] that has such good success with diatomic examples.

Without offering an answer or physical insight to this question, the theoretical treatment of glyoxal scattering bears on the issue.[6−8,11] The H_2 and He predictions displayed in Figure 6 were carried out for the actual E_{cm} of our experiments. In contrast, those for Ar were performed[7] for $E_{cm} = 650$ cm^{-1} (80 meV), an energy far below the $E_{cm} = 2000$ cm^{-1} of our actual experiment. Despite the kinematic mismatch between the calculations and experiment, the predictions shown in Figure 6 fit the experimental rotational distribution to within the error bars. Thus, the message relayed by the scattering calculations echoes that of the experiment; the distribution of rotationally inelastic cross sections is surprisingly insensitive to the kinematic details of the collision, at least for these high collision energies.

The exponential gap law representation of rotational cross section distributions introduced by Polanyi and Woodall[46] to describe early HF data has evolved into elaborate theoretical and experimental discussions of fitting and scaling laws.[47] Without attempting to establish any scaling or fitting parameters for glyoxal experiments, the possibility of fitting the cross sections with a simple exponential gap law is explored in Figure 7. It is seen that EGL fitting based on angular momentum transfer (ΔK) is reasonably successful, whereas EGL fitting based on energy transfer (ΔE) is less appropriate. The central role of angular momentum in rotationally inelastic scattering has been extensively discussed,[12,44,45,47,48] and it forms the basis[49] of the energy corrected sudden (ECS) scaling laws that have had considerable success in the treatment of rotationally inelastic scattering of diatomic molecules from rare gases.[12]

The fall off of cross sections for $\Delta K \gtrsim 10$ for H_2 and He is probably the only opportunity in our data to detect limits on rotationally inelastic scattering imposed by the collisional kinematics. It is instructive to explore the respective rolls of collisional energy and collisional angular momentum as limiting factors. Orbital angular momentum considerations have been discussed earlier in some detail in conjunction with scattering of glyoxal by H_2[1]. For the present purposes, it is sufficient to calculate the approximate orbital angular momentum L available to the collision pair from the classical expression $L = \mu v b$, where μ is the reduced mass, v is the center of mass velocity, and b is the impact parameter. An approximate upper limit is obtained if one assumes that the probability of inelastic scattering falls off rapidly for collisions with impact parameters beyond the geometric boundaries established by the H and O atoms that lie 1.6 and 1.7 Å from the glyoxal center of mass. The values so calculated are listed in Table 1 along with the appropriate center of mass velocities. The table also contains the minimum rotational energy of the K' states, as calculated for $J = K$.

The limiting orbital angular momentum values $L \approx 14\hbar$ and $21\hbar$ for H_2 and He, respectively, are close to the maximum $\Delta K' \approx 15$ observable in our experiments for each gas (Figure 7). Since the available collision energy is well above that needed to reach these rotational states, the fall off in cross sections at large ΔK appears to be a consequence of angular momentum constraints rather than E_{cm} limitations.

The story differs for Ne and the heavier gases. In these cases, the systems run out of collision energy long before reaching their angular momentum limits. For example, the orbital angular momentum limit of $L \approx 100\hbar$ for scattering by neon corresponds to a rotational level $K = J \approx 100$ whose energy is about 19 600 cm^{-1} above the initial level, 0^0K^0. In contrast the glyoxal−neon collision energy $E_{cm} \approx 1400$ cm^{-1} corresponds to excitation of $K \approx 27$, far below the limit imposed by the orbital angular momentum.

Rotationally inelastic scattering to levels near the E_{cm} limit cannot be observed experimentally for Ne and the heavier gases. The observational cutoff at $K = 21$ for Ne occurs when the rotational cross sections become too small to be resolved in the midst of the rovibrational inelastic scattering. For example, the ^rR sub-bandhead of 0^0K^{21} emission is overlapped by sub-bandheads from 7^1K.[5,6] The rotational and rovibrational cross sections for scattering to these levels are of comparable magnitude, and beyond $\Delta K = 21$, the rotationally inelastic scattering by Ne becomes too small to measure.

Rotational cross sections for Ar, Kr, and Xe are reported to $K = 26$ which is the limit of our spectroscopic search. As can be seen in Figure 7 or Table 2, cross sections for scattering with $\Delta K \approx 20-26$ have fallen to about 2% of the largest observed rotationally inelastic cross section ($\Delta K = 3$), and their scaling against ΔE has begun to level off.

Acknowledgment. We greatly appreciate the helpful interactions with Dr. Miles Weida concerning the spectral simulations and with Prof. A. J. McCaffery. Financial support was provided by the National Science Foundation and by the donors of the Petroleum Research Foundation administered by the American Chemical Society.

References and Notes

(1) Butz, K. W.; Du, H.; Krajnovich, D. J.; Parmenter, C. S. *J. Chem. Phys.* **1988**, *89*, 4680.

(2) Gilbert, B. D.; Parmenter, C. S.; Krajnovich, D. J. *J. Phys. Chem.* **1994**, *98*, 7116.
(3) Gilbert, B. D.; Parmenter, C. S.; Krajnovich, D. J. *J. Chem. Phys.* **1994**, *101*, 7423.
(4) Gilbert, B. D.; Parmenter, C. S.; Krajnovich, D. J. *J. Chem. Phys.* **1994**, *101*, 7440.
(5) Parmenter, C. S.; Clegg, S. M.; Krajnovich, D. J.; Lu, S.-P. *Proc. Natl. Acad. Sci. U.S.A.* **1997**, *94*, 8387.
(6) Clary, D. C.; Dateo, C. E. *Chem. Phys. Lett.* **1989**, *154*, 62.
(7) Kroes, G.-J.; Rettschnick, R. P. H.; Dateo, C. E.; Clary, D. C. *J. Chem. Phys.* **1990**, *91*, 287.
(8) Kroes, G.-J.; Rettschnick, R. P. H. *J. Chem. Phys.* **1991**, *94*, 360.
(9) Krajnovich, D. J.; Butz, K. W.; Du, H.; Parmenter, C. S. *J. Chem. Phys.* **1989**, *92*, 7705.
(10) Birss, F. W.; Brown, J. M.; Cole, A. R. H.; Lofthus, A.; Krishanamachari, S. L. N. G.; Osborne, G. A.; Paldus, J.; Ramsay, D. A.; Watmann, L. *Can. J. Phys.* **1970**, *48*, 1230.
(11) Kroes, G.-J.; Rettschnick, R. P. H.; Clary, D. C. *Chem. Phys.* **1990**, *148*, 359.
(12) Dexheimer, S. L.; Durand, M.; Brunner, T. A.; Pritchard, D. E. *J. Chem. Phys.* **1982**, *76*, 4996.
(13) Steinfeld, J. I.; Klemperer, W. *J. Chem. Phys.* **1965**, *42*, 3475.
(14) Scott, T. P.; Smith, N.; Pritchard, D. E. *J. Chem. Phys.* **1984**, *80*, 4841.
(15) Islam, M.; Smith, I. W. M.; Wiebrecht, J. W. *J. Chem. Phys.* **1995**, *103*, 9676.
(16) Smith, A. V.; Johnson, A. W. *Chem. Phys. Lett.* **1982**, *93*, 608.
(17) Imajo, T.; Shibuya, K.; Obi, K. *Chem. Phys. Lett.* **1987**, *137*, 139.
(18) Meyer, H. *J. Chem. Phys.* **1995**, *102*, 3151.
(19) Chapman, W. B.; Weida, M. J.; Nesbitt, D. J. *J. Chem. Phys.* **106** 1997.
(20) Fei, R.; Lambert, H. M.; Carrington, T.; Filseth, S. V.; Sadowski, C. M.; Dugan, C. H. *J. Chem. Phys.* **1994**, *100*, 1190.
(21) Fei, R.; Adelman, D. E.; Carrington, T.; Dugan, C. H.; Filseth, S. V. *Chem. Phys. Lett.* **1995**, *232*, 547.
(22) Davis, S. J.; Holtzclaw, K. W. *J. Chem. Phys.* **1990**, *92*, 1661.
(23) Wolf, P. J.; Davis, S. J. *J. Chem. Phys.* **1987**, *87*, 3492.
(24) Brunner, T. A.; Smith, N.; Karp, A. W.; Prichard, D. E. *J. Chem. Phys.* **1981**, *74*, 3324.
(25) Brunner, T. A.; Driver, R. D.; Smith, N.; Pritchard, D. E. *J. Chem. Phys.* **1979**, *70*, 4155.
(26) Brunner, T. A.; Driver, R. D.; Smith, N.; Pritchard, D. E. *Phys. Rev. Lett.* **1978**, *41*, 856.
(27) Serri, J. A.; Morales, A.; Moskowitz, W.; Prichard, D. E.; Becker, C. H.; Kinsey, J. L. *J. Chem. Phys.* **1980**, *72*, 6304.
(28) Serri, J. A.; Bilotta, R. M.; Prichard, D. E. *J. Chem. Phys.* **1982**, *77*, 2940.
(29) Brechignac, P.; Whitaker, B. J. *Chem. Phys.* **1984**, *88*, 425.
(30) Ziegler, G.; Kumar, S. V. K.; Rubahn, H. G.; Kuhn, A.; Sun, B.; Bergmann, K. *J. Chem. Phys.* **1991**, *94*, 4252.
(31) Schiffman, A.; Chandler, D. W. *Int. Rev. Phys. Chem.* **1995**, *14*, 371.
(32) Buck, U.; Kohl, K. H.; Kohlhase, A.; Faubel, M.; Staemmler. *Mol. Phys.* **1985**, *55*, 1255.
(33) Chapman, W. B.; Schiffman, A.; Hutson, J. M.; Nesbitt, D. J. *J. Chem. Phys.* **1996**, *105*, 3497.
(34) Buck, U.; Kohlhase, A.; Secrest, D.; Phillips, T.; Scoles, G.; Grein, F. *Mol. Phys.* **1985**, *55*, 1233.
(35) Schiffman, A.; Chapman, W. B.; Nesbitt, D. J. *J. Phys. Chem.* **1996**, *100*, 3402.
(36) Nesbitt, D. J.; Nibler, J. W.; Schiffman, A.; Chapman, W. B. *J. Chem. Phys.* **1993**, *98*, 9513.
(37) Buck, U.; Kohlhase, A.; Phillips, T.; Secrest, D. *Chem. Phys. Lett.* **1983**, *98*, 199.
(38) Oka, T. *J. Chem. Phys.* **1968**, *49*, 3135.
(39) Oka, T. *J. Chem. Phys.* **1967**, *47*, 4852.
(40) Abel, B.; Coy, S. L.; Klaassen, J. J.; Steinfeld, J. I. *J. Chem. Phys.* **1992**, *96*, 8236.
(41) Schleipen, J.; ter Meulen, J. J. *Chem. Phys.* **1991**, *156*, 479.
(42) Schleipen, J.; ter Meulen, J. J.; Offer, A. R. *Chem. Phys.* **1993**, *171*, 347.
(43) Schleipen, J.; ter Meulen, J. J.; van der Sanden, G. C. M.; Wormer, P. E. S.; van der Avoird, A. *Chem. Phys.* **1992**, *163*, 161.
(44) Osborne, M. A.; McCaffery, A. J. *J. Chem. Phys.* **1994**, *101*, 5604.
(45) McCaffery, A. J.; Alwahabi, Z. T.; Osborne, M. A.; Williams, C. J. *J. Chem. Phys.* **1993**, *98*, 4586.
(46) Polanyi, J. C.; Woodall, K. B. *J. Chem. Phys.* **1972**, *56*, 1563.
(47) Brunner, T. A.; Pritchard, D. In *Dynamics of the Excited State*; Lawley, K. P., Ed.; John Wiley & Sons: New York, 1982; Vol. L, p 589.
(48) Ewing, G. E. *J. Phys. Chem.* **1987**, *91*, 4662.
(49) DePristo, A. E.; Augustin, S. D.; Ramasmany, R.; Rabitz, H. *J. Chem. Phys.* **1978**, *71*, 850.